WAKEFIELD EFFECTS OF NEW ILC CAVITY SHAPES*

FERMILAB-PUB-06-549-APC

Igor Zagorodnov#, DESY, Hamburg, Germany
Nikolay Solyak, Fermilab, Batavia, Illinois, USA

Abstract

The operation of the International Linear Collider (ILC) requires high gradients and quality factors in the accelerating structure. One way to reach it is to modify the cavity shape to reduce the ratio of peak surface magnetic to accelerating field. Two candidate shapes are suggested recently: the Re-entrant shape [1] and the Low-Loss shape [2]. To get the maximum advantages of a new cavity shape it was proposed also to reduce the iris aperture from original 70 mm in the TESLA cavity to 66 mm in the Re-entrant cavity and 60 mm in the Low Loss cavity [2]. The expected effect of aperture reduction on the amplitude of short-range wakefields is bigger than the effect of the cavity shape itself. In this paper we estimate numerically longitudinal and transverse short range wake functions for the new shapes, recently proposed in paper [2]. The obtained analytical expressions are used in beam dynamic simulations for ILC lattice. We show that ILC will tolerate the cavities with the new shapes and the smaller iris diameter.

INTRODUCTION

In order to reach higher gradients several modified cavity shapes are suggested recently [2] for the ILC project. In this paper we estimate numerically the longitudinal and the transverse wake functions for Re-entrant (RE) and Low-Loss (LL) shapes following ideas developed earlier in [3, 4]. Using a time domain numerical approach [5, 6], we calculate the short-range wakefields in the accelerating structure of two cryomodules with a total length of ~24m. The wakepotentials are calculated for bunches of different length. The numerical results are fitted to analytical estimations [8] and explicit expressions for monopole and dipole wake functions are derived.

The obtained analytical expressions are used in beam dynamic simulations for the ILC lattice, which show that the ILC will tolerate the cavities with the new shapes and the smaller iris diameter.

WAKE FUNCTIONS FOR ILC ACCELERATING STRUCTURE

Analytical estimations

We consider an axially symmetric structure and a bunch with a charge of Q moving parallel to the axis. The bunch with a longitudinal distribution $q(s)$ travels near the axis, and thus the longitudinal loss is dominated by monopole fields

$$L_{\|} \cong \left\langle W_{\|}^{0} \right\rangle = \frac{1}{Q}\int_{-\infty}^{\infty} W_{\|}^{0}(s)q(s)ds = \frac{1}{Q^2}\int_{-\infty}^{\infty}\int_{-\infty}^{s} w_{\|}^{0}(s-s')q(s')q(s)ds'ds$$

and the transversal kick by dipole fields

$$L_{\perp} \cong \left\langle W_{\perp}^{1} \right\rangle = \frac{1}{Q}\int_{-\infty}^{\infty} W_{\perp}^{1}(s)q(s)ds = \frac{1}{Q^2}\int_{-\infty}^{\infty}\int_{-\infty}^{s} w_{\perp}^{1}(s-s')q(s')q(s)ds'ds\,.$$

Short bunches interact with single cavity and periodical structure in a different way. However, in both cases the wake functions $w_{\|}^{0}(s)$ and $w_{\perp}^{1}(s)$ at short distance s are approximately related by simple equation [8]

$$\partial_s w_{\perp}^{1}(0) = \frac{2}{a^2} w_{\|}^{0}(0)\,, \qquad (1)$$

where a is the iris radius.

In the periodic structure the short range wake functions can be approximated by the relations [8]

$$w_{\|}(s) = L\frac{Z_0 c}{\pi a^2}\exp(-\sqrt{s/s_0})\,, \qquad (2)$$

$$w_{\perp}(s) = \frac{2}{a^2} w_{\|}(0) 2s_1\left(1-\left(1+\sqrt{s/s_1}\right)\exp(-\sqrt{s/s_1})\right), \qquad (3)$$

where L, s_0, s_1 are fit parameters to be defined.

Numerical calculations

The ILC linac consists of a long chain of cryomodules. One cryomodule with a total length of 12 m contains 8 cavities and 9 bellows [4]. The geometry of the new cavity shapes is shown in Fig. 1. The iris radius is equal to 33 mm for RE shape and it is equal to 30 mm for LL shape.

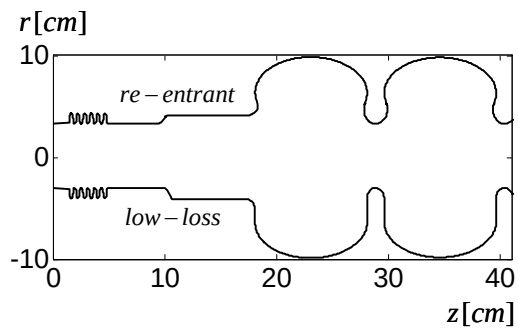

Figure 1: The geometry of the new shapes.

The wakefields for Gaussian bunches up to $\sigma = 100\,\mu\text{m}$ are studied. To reach a steady state solution a structure of two cryomodules with a total length of 24m was studied.

The ILC linac can be considered as a multi-periodic structure. The first elementary period is the cavity cell, the second one is the 9-cell cavity with a bellow and beam tubes and the third one is the cryomodule, housing 8 cavities with 9 bellows.

*Work supported in part by EUROFEL project
#igor.zagorodnov@desy.de

The new cavity shapes have smaller iris radii compared with the TESLA shape. As expected it results in stronger wake field effects.

From the fit of the numerical data for the RE shape to equations (2), (3) we obtain

$$w_{\|}(s) = -388\exp(-\sqrt{s/s_0})[\text{V/pC/module}],$$

$$w_{\perp}(s) = 1300\left(1-\left(1+\sqrt{\frac{s}{s_1}}\right)\exp\left(-\sqrt{\frac{s}{s_1}}\right)\right)\left[\frac{\text{V}}{\text{pC}\times\text{m}\times\text{module}}\right],$$

where $s_0 = 1.9\cdot 10^{-3}$ and $s_1 = 0.91\cdot 10^{-3}$.

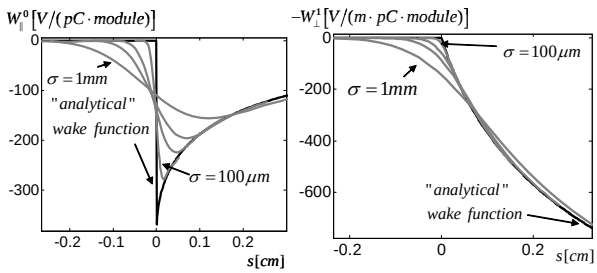

Figure 2: The numerical wakes and the analytical wake functions for Re-entrant shape.

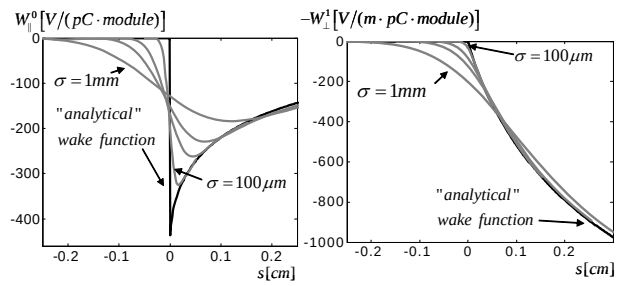

Figure 3: The numerical wakes and the analytical wake functions for the Low-Loss shape.

From comparison of these expressions with (2), (3) we find that they fit, if we define an "effective length" for the cryomodule as $L = 11.76$ m and take an iris radius $a = 33$ mm.

Fig. 2 shows the numerical (gray dashed lines) wake potentials for bunches with a RMS length $\sigma = 100$, 500, 300, 100 μm. The derived analytical wake functions are shown by solid black lines.

From the fit of the numerical data for the LL shape to equations (2), (3) we obtain the wake functions

$$w_{\|}(s) = -459\exp(-\sqrt{s/s_0})[\text{V/pC/module}],$$

$$w_{\perp}(s) = 1720\left(1-\left(1+\sqrt{\frac{s}{s_1}}\right)\exp\left(-\sqrt{\frac{s}{s_1}}\right)\right)\left[\frac{\text{V}}{\text{pC}\times\text{m}\times\text{module}}\right],$$

where $s_0 = 1.85\cdot 10^{-3}$ and $s_1 = 0.84\cdot 10^{-3}$. The last expressions fit to formulas (2), (3) with an iris radius $a = 30$ mm and an "effective length" of the cryomodule $L = 11.5$ m.

Like in the periodic case the longitudinal wake functions scale as $O(1), s \to 0$ and the transversal wake functions scale as $O(s)$, $s \to 0$.

Fig. 3 shows the numerical (gray dashed lines) wake potentials for bunches with $\sigma = 100$, 500, 300, 100 μm. The analytical wake functions are represented by solid black lines.

To obtain the formulas for the wake function on the unit of active length the above relations should be divided by "active" length $L_a = 8.288$ [m/module].

Fig. 4 compares the wake functions obtained in this paper with the earlier calculated results for the TESLA shape [4]:

$$w_{\|}(s) = -344\exp(-\sqrt{s/s_0})[\text{V/pC/module}],$$

$$w_{\perp}(s) = 1000\left(1-\left(1+\sqrt{\frac{s}{s_1}}\right)\exp\left(-\sqrt{\frac{s}{s_1}}\right)\right)\left[\frac{\text{V}}{\text{pC}\times\text{m}\times\text{module}}\right],$$

where $s_0 = 1.74\cdot 10^{-3}$ and $s_1 = 0.92\cdot 10^{-3}$.

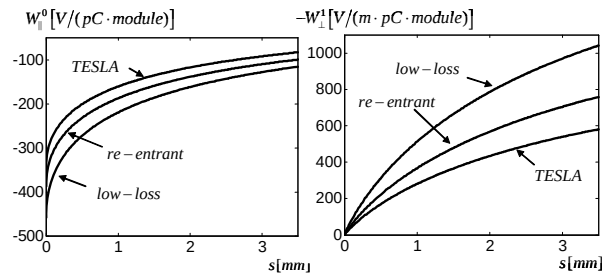

Figure 4: The wake functions for different cavity shapes.

BEAM DYNAMIC SIMULATIONS

The ILC Baseline Configuration Document accepts the TESLA cavity shape as a basic choice. The accelerating cavities with RE and LL shape are considered as alternatives, which will improve the cavity performances. One of the concerns of the alternative designs are larger short-range wakefields and, as a result, a higher emittance growth in the ILC linac. To understand this effect a series of beam dynamic simulations has been done for all three cavity shapes.

The linac cryogenic system is divided into cryomodules (CM) with 8 cavities per CM. The accelerating gradient is 31.5 MV/m with the beam phase of 5º off-crest. The magnet optics: a regular FODO lattice with one quad for four CM's and the phase advance of 75º / 60º in x/y plane. Each quad has an attached cavity style BPM and a vertical corrector. The horizontal corrector is attached to the horizontally focusing quads only. Geometrically, the linac follows to the Earth curvature. In the main linac the beam is accelerated from 15 GeV to 250 GeV. All elements are initially misaligned according to Table 1 [10]. Beam Dynamic Simulations were done by using MatLIAR code [13], modified for the curved linac.

Two different beam based alignment (BBA) techniques were used to align the machine: one-to-one (or flat) steering and the following Dispersion Free Steering

(DFS) [11]. For BBA steering the linac was divided into few segments (not the same segmentation for flat and DFS). In flat steering each segment was iteratively aligned by minimizing the RMS value of the BPM readings. The DFS technique was applied to the linac after the flat steering. In each of them the difference between two orbits (beam with nominal and reduced energies) and the RMS beam offset in the BPM's were minimized simultaneously. Several iterations have been done before going to the next segment. For statistics the simulations were performed for 50 seeds (with different initial alignments). The first seven BPM's (launch region) were aligned with 30 µm RMS offset, since we didn't explore the beam energy variation at the linac entrance needed for the DFS.

Table 1. Nominal misalignment.

Tolerance	Vertical plane
BPM Offset w.r.t. Cryostat	300 µm
Quad offset w.r.t. Cryostat	300 µm
Quad Rotation w.r.t. Cryostat	300 µrad
Cavity Offset w.r.t. Cryostat	300 µm
Cryostat Offset w.r.t. Survey Line	200 µm
Cavity Pitch w.r.t. Cryostat	300 µrad
Cryostat Pitch w.r.t. Survey Line	20 µrad
BPM Resolution	1.0 µm

The results of the emittance growth in the linac built out of cavities with different shapes are shown in Fig. 5. The vertical normalized emittance (corrected to remove the beam dispersion) is plotted as a function of BPM index along the linac. Each curve represents the mean value of 50 seeds. The initial normalized emittance was 20 nm and the beam energy spread was 150 MeV. As one can see here, the emittance growth for LL cavities is almost twice higher than for TESLA cavities. It is close to the allowed emittance budget for the linac: 30 nm. Other sources of emittance growth like quadrupoles, correctors and beam jitters were not taken into account.

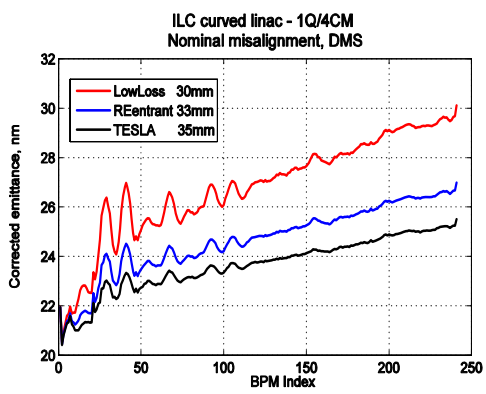

Figure 5: Emittance dilution along the curved ILC linac for cavities with different shapes and apertures: TESLA, RE33 and LL30.

For the TESLA style cavities the wakefields are responsible for ~1/3 of the emittance growth in the linac. In the case of LL30 cavities the emittance dilution is dominated by the wakefields. This result of the BBA can be improved by better cavities alignment (for example, 200 µm initial misalignment instead of nominal 300 µm (see Fig.6)). Another effective way to reduce the emiitance dilution in the ILC main linac is the implementation of additional correcting knobs - dispersion and wakefield bumps [11-12].

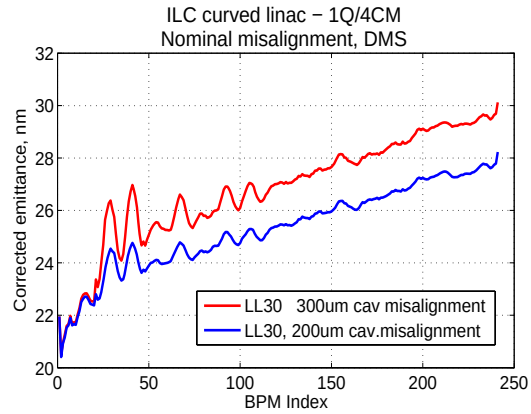

Figure 6: Effect of cavity initial misalignments on emittance dilution in the linac with LL type cavities.

Simulations of static tuning by using bumps are underway.

ACKNOWLEDGEMENTS

The authors thank K. Bane, M. Dohlus, T. Weiland, K. Ranjan, A. Valishev, P. Tenenbau for helpful discussions.

REFERENCES

[1] V. Shemelin, H. Padamsee, R.L. Geng, Nucl. Instr. and Meth.in Phys. Res. A, 496 (2003).
[2] J. Sekutowicz, "Design of a Low Loss SRF cavity for the ILC", PAC'05, Knoxville, May 2005, p.3342.
[3] A. Novokhatski, M. Timm, T. Weiland, DESY TESLA-99-16, 1999.
[4] I. Zagorodnov, T. Weiland, "The short-range transverse wakefields in TESLA accelerating structure ", PAC'03, Portland, May 2003, p.3249.
[5] S. Novokhatski, SLAC–PUB–11556, 2005.
[6] I. Zagorodnov, T. Weiland, PR-STAB 8 (2005).
[7] A.V. Fedotov, R.L. Gluckstern, M. Venturini, Phys. Rev. STAB 2 (1999).
[8] K.L.F. Bane, SLAC-PUB-9663, LCC-0116, 2003.
[9] K.L.F. Bane, M. Sands, SLAC-PUB-4441,1987.
[10] http://ilc-dms.fnal.gov/ embers/kirti/Mar_2906_talk/ ILCMainLinac.ppt
[11] T. Raubenheimer, P. Tenenbaum, SLAC-TN-03-071, LCC-0129, 2004.
[12] P. Eliasson, D. Schulte, PAC'05, 2005, p.1141-1143.
[13] http://www.slac.stanford.edu/accel/nlc/local/Accel Physics/codes/liar/web/liar.htm